International Journal of Mechanical, Industrial and Aerospace Sciences
ISSN: 2517-9950
Vol:10, No:7, 2016

Inverse Heat Transfer Analysis of a Melting Furnace Using Levenberg-Marquardt Method

Mohamed Hafid, Marcel Lacroix

***Abstract*—**This study presents a simple inverse heat transfer procedure for predicting the wall erosion and the time-varying thickness of the protective bank that covers the inside surface of the refractory brick wall of a melting furnace. The direct problem is solved by using the Finite-Volume model. The melting/solidification process is modeled using the enthalpy method. The inverse procedure rests on the Levenberg-Marquardt method combined with the Broyden method. The effect of the location of the temperature sensors and of the measurement noise on the inverse predictions is investigated. Recommendations are made concerning the location of the temperature sensor.

***Keywords*—**Melting furnace, inverse heat transfer, enthalpy method, Levenberg–Marquardt Method.

I. Introduction

MELTING furnaces, such as electric arc furnaces (Fig. 1), are used for material processing that requires high powers and elevated temperatures. Their main applications are the smelting of materials such as copper, steel and nickel calcine. An interesting solid/liquid phase change phenomenon that arises in these melting furnaces is the formation of solid layer, called a bank, that covers the inside surface of the refractory brick wall. This bank plays a crucial role in these furnaces. It protects the brick walls from the highly corrosive molten bath. Keeping a bank of optimal size is therefore crucial for the safe and profitable operation of the smelting furnace. It is very difficult to measure the bank thickness using probes submerged into the molten bath. The hostile conditions that prevail in the melt damage the probes and may even destroy them. This method is time consuming, risky and often inaccurate. Moreover, formation of the bank is the most complex process that depends on the boundary conditions.

In recent years, the problem of bank formation inside high-temperature melting furnaces has been tackled with various inverse heat transfer methods such as the Levenberg-Marquardt method [1], the Kalman-filter method [2]-[6] and the conjugate gradient method with the adjoint equation [7]-[10]. In all the aforementioned studies, the focus is on the inverse prediction of the time-varying heat load of the furnace i.e. the heat flux q"(t) at ($x=L_{Brick} + L_{PCM}$) (Fig. 2). Once the heat load is determined, the time-varying bank thickness $E(t)$ that covers the inside surface of the refractory brick wall can be calculated.

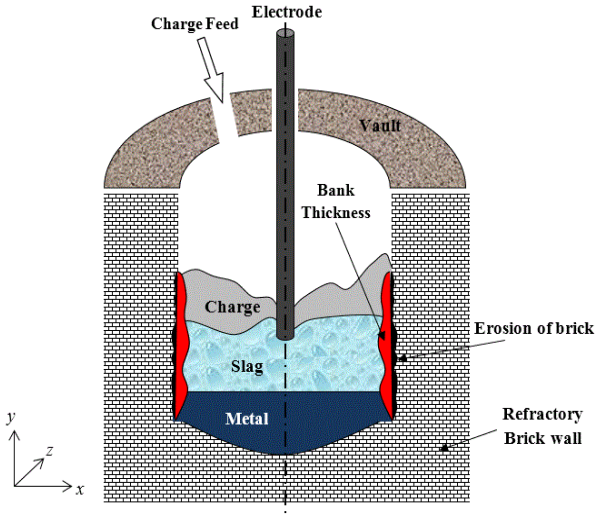

Fig. 1 Cross view of a typical melting furnace

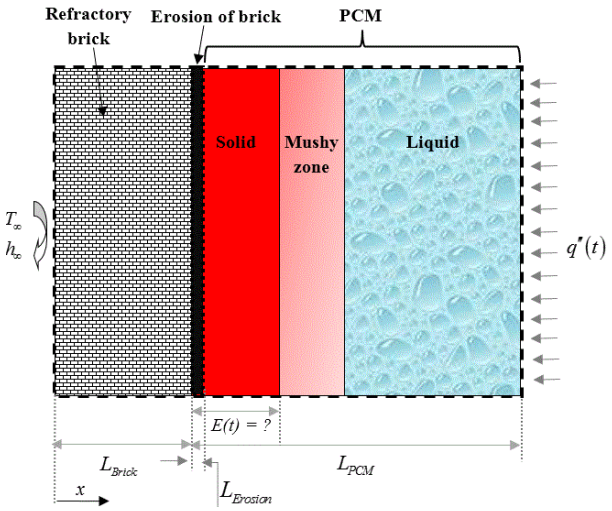

Fig. 2 Schematic of the direct problem. $E(t)$ is unknown. It is predicted numerically with the FVM

Another problem that arises inside these furnaces is the erosion-corrosion of the inner surface of the refractory brick wall. This problem occurs when the bank is lost and the inside lining of the wall suddenly becomes exposed to the hostile molten material. Predicting the erosion-corrosion wear is a crucial factor for determining the active life of the furnace.

Hafid M. is with the Department of Mechanical Engineering, Université de Sherbrooke, 2500 Blvd. de l'Université, Sherbrooke (Québec) J1K 2R1, Canada (phone: (873) 888-7768, e-mail: mohamed.hafid@usherbrooke.ca).
Lacroix M. is with the Department of Mechanical Engineering, Université de Sherbrooke, 2500 Blvd. de l'Université, Sherbrooke (Québec) J1K 2R1, Canada (phone: (819)821-8000 poste 62145, e-mail: Marcel.Lacroix@uSherbrooke.ca).

But, this task is very challenging due to the physical and chemical conditions that prevail inside the furnace [11], [12].

In the present study, an inverse heat transfer procedure is proposed for predicting simultaneously the erosion-corrosion thickness $L_{Erosion}$ with the unknown time-varying heat flux q"(t). Once these parameters are estimated, the time-varying protective PCM bank that coats the internal surface of the furnace wall can be predicted. The solid/liquid phase change problem is modeled with the enthalpy method. The inverse problem is handled with the Levenberg-Marquardt Method (LMM) combined to the Broyden method (BM).

II. Finite-Volume Model (FVM) of The Melting Furnaces

Fig. 2 shows a schematic of the 1-D non-isothermal phase change problem. Here, the PCM is composed of a solid layer, a mushy zone and liquid layer. The inner surface of the refractory brick wall is covered by a protective bank whose time-varying thickness is *E(t)*. *E(t)* shows the position of the solidification front of the PCM.

The mathematical model for the melting furnace rests on the following assumptions [2]-[7], [9]:

- ✓ The temperature gradients in the *x* direction are much larger than those in the other directions. Consequently, a one-dimensional analysis can be applied (Fig. 2).
- ✓ The thermal contact resistance between the refractory brick wall and the PCM is neglected.
- ✓ The heat transfer inside the liquid phase of the PCM is conduction dominated [7], [13].
- ✓ The thermal properties of the phase change material (PCM) are temperature independent.
- ✓ The phase change problem is non-isothermal. The PCM is depicted by three zones: a solid phase, a mushy zone and a liquid phase (Fig. 2).

The governing heat diffusion equation for the refractory brick wall and the PCM is expressed as

$$\rho C_p \frac{\partial T}{\partial t} = \frac{\partial}{\partial x}\left(k \frac{\partial T}{\partial x} \right) - \delta H \frac{\partial f}{\partial t} \tag{1}$$

Where δH and f are the enthalpy and the liquid fraction, respectively. The enthalpy δH is defined as

$$\delta H = \rho (C_{p,liquid} - C_{p,solid}) T + \rho \lambda \tag{2}$$

The liquid fraction f is given by

$$f = F(T) = \begin{cases} 0 & T \le T_{sol} \quad (Solid \text{ region}) \\ \dfrac{T - T_{sol}}{T_{liq} - T_{sol}} & T_{sol} \le T \le T_{liq} \quad (Mushy \text{ region}) \\ 1 & T \ge T_{liq} \quad (Liquid \text{ region}) \end{cases} \tag{3}$$

The liquid fraction f is updated iteratively at each time-step in the following manner [16]

$$f^{k+1} \approx f^k + \left(\frac{dF}{dT} \right)^k \left(T^{k+1} - F^{-1}\left(f^k \right) \right) \tag{4}$$

F^{-1} is the inverse function of F. The boundary conditions at the left and at the right (Fig. 2) are:

$$\begin{cases} \left(k \dfrac{\partial T}{\partial x} \right)_{x=0} = h_\infty \left(T(0,t) - T_\infty \right) \\ \left(k \dfrac{\partial T}{\partial x} \right)_{x=L_{Brick}+L_{PCM}} = q''(t) \end{cases} \tag{5}$$

Equations (1)-(5) are solved numerically by using a time-implicit finite-volume method. The resulting set of algebraic equations is then solved by using the Tri-Diagonal-Matrix-Algorithm (TDMA).

The accuracy of the FVM was first validated by using the one-dimensional solidification of the binary Al–4,5% Cu alloy with properties reported in [15], [16]. A Dirichlet boundary condition of T=573 K is assumed at the boundary $x=L_{Brick}$ (Fig. 2). The width of the PCM layer is set equal to L_{PCM}=0,5 m and the initial temperature is set equal to T_{in}= 969 K.

The predicted liquidus and solidus fronts are presented in Fig. 3. It is seen that the predictions of the present model (FVM) are in excellent agreement with the semianalytical heat balance integral method [15] and the source-based numerical method [16].

III. The Direct Model

For the direct problem, all the physical and the geometrical properties are known. The objective of the direct model is to determine the temperature field *T(x,t)* and the time-varying thickness of the protective bank *E(t)* using the FVM presented above.

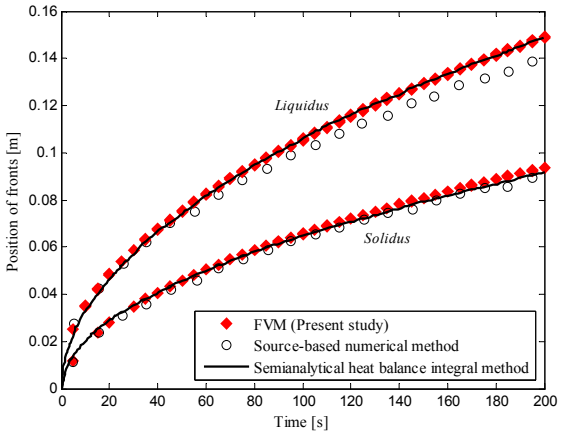

Fig. 3 Solidification of a binary Al–4,5%-Cu alloy: Comparison with the results reported in [15], [16]

The direct model was implemented for the entire melting furnace i.e. the refractory brickwall and the PCM. The operating thermal conditions of the furnace are similar to those

reported in [2], [3]. The refractory brick wall is set equal to L_{Brick}=0,1 m and the PCM layer (solid, mushy, and liquid) is set equal to L_{PCM}=0,1 m (Fig. 2). The external temperature is set equal to T_∞=300 K and the outside average heat transfer coefficient is fixed at h_∞=15 W/m^2. K. At $x=L_{Brick} + L_{PCM}$, the time-varying heat flux q"(t) is given by

$$q''(t) = P_1 + P_2 * \sin^2\left(\frac{2\pi . t}{t_{\max}}\right) \quad (6)$$

When the protective bank is lost, the inside surface of the refractory brick wall suddenly comes into direct contact with the molten material. Consequently, the exposed brick wall is attacked and becomes vulnerable to erosion-corrosion.

Indeed, erosion of refractory brick walls is a slow process [17], [18]. Therefore, the eroded portion of the wall may be considered time-independent within the time-intervals simulated here, $t \in [0,\ 400000]$ s. The eroded portion of the refractory wall $L_{Erosion}$ is set to

$$L_{Erosion} = 0,01\ (m) = P_3 \quad (7)$$

The coefficients are given by

$$\begin{cases} P_1 = 9000 & (\mathrm{W/m^2}) \\ P_2 = 8000 & (\mathrm{W/m^2}) \\ P_3 = 0,01 & (m) \end{cases} \quad (8)$$

The thermophysical properties of the melting furnace (brick wall and PCM) are summarized in Table I [2], [3].

All numerical simulations were conducted with a grid size of 200 uniformly distributed control volumes inside the PCM layer and the refractory brick wall. The time step was set equal to 100 s.

TABLE I
THERMO PHYSICAL PROPERTIES OF THE REFRACTORY BRICK WALL AND OF THE PCM [2], [3]

Parameter	Value	Unit
k_{BRICK}	16,8	(W/m K)
$C_{p,BRICK}$	875	(J/kg K)
ρ_{BRICK}	2600	(kg/m^3)
$k_{PCM,solid}$	1	(W/m K)
$k_{PCM,liquid}$	100	(W/m K)
$C_{p,PCM,solid}$	1800	(J/kg K)
$C_{p,PCM,liquid}$	1800	(J/kg K)
ρ_{PCM}	2100	(kg/m^3)
λ_{PCM}	5,1 x 105	(J/kg)
T_{sol}	1213	K
T_{liq}	1233	K

IV. THE INVERSE MODEL

For the inverse problem, it is assumed that the time-varying heat flux (at $x=L_{Brick} + L_{PCM}$) and the thickness of the eroded wall ($L_{Erosion}$) are unknown; i.e., P_1, P_2, and P_3 are unknown. The objective of the inverse analysis is to determine the unknown thermal parameters by using temperature measurements taken from a sensor located inside brick wall (Fig. 4). Once the time-varying heat flux q"(t) and the thickness of the eroded wall $L_{Erosion}$ are determined, the time-varying thickness $E(t)$ of the protective bank may be estimated from the direct model (FVM) presented above.

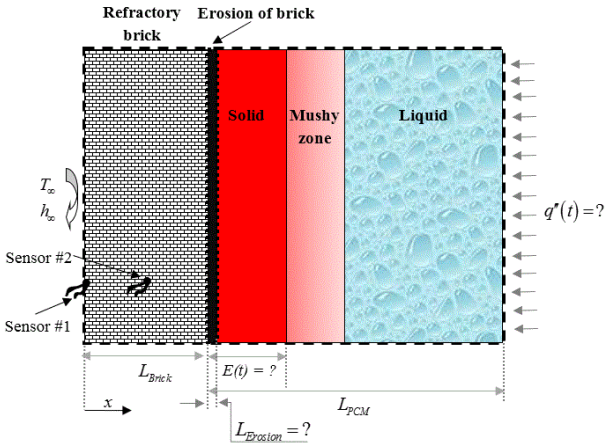

Fig. 4 The inverse problem. q"(t) and $L_{Erosion}$ are unknown. They are determined from sensor#1 or sensor#1

The solution for the inverse problem consists of minimizing the least square norm $\Psi(\vec{P})$:

$$\Psi(\vec{P}) = \sum_{i=1}^{I}\left[Y(t_i) - \hat{T}(t_i, \vec{P})\right]^2 \quad (9)$$

where $P= (P_1, P_2, P_3)$ is the set of the unknown parameters. Here $Y(t_i)$ are the temperatures measured i.e. temperatures generated from the solution of the direct problem wherein the parameters vector $P= (P_1, P_2, P_3)$ are known. $\hat{T}(t_i, \vec{P})$ are the estimated temperatures from the inverse model. I is the total number of measurements.

The inverse problem is solved with the Levenberg–Marquardt Method (LMM). The incremental value of the unknown parameters ΔP, is given by:

$$\Delta\vec{P} = \left[\left(\vec{J}^k\right)^T \vec{J}^k + \mu^k \vec{\Omega}^k\right]^{-1} \left(\vec{J}^k\right)^T \left(\vec{Y} - \vec{T}\left(\vec{P}^k\right)\right) \quad (10)$$

Here μ^k is a positive damping parameter. The choice and the update of this parameter is discussed in [19]. $\vec{\Omega}^k = diag\left[\left(\vec{J}^k\right)^T \vec{J}^k\right]$ is a diagonal matrix. The superscript

"T" denotes the transpose of the matrix. $\vec{\vec{J}}^k$ is the Jacobian matrix and it is defined as

$$\vec{\vec{J}}\left(\vec{P}\right)=\begin{pmatrix}\frac{\partial T_1}{\partial P_1} & \frac{\partial T_1}{\partial P_2} & \frac{\partial T_1}{\partial P_3}\\ \frac{\partial T_2}{\partial P_1} & \frac{\partial T_2}{\partial P_2} & \frac{\partial T_2}{\partial P_3}\\ \vdots & \vdots & \vdots\\ \frac{\partial T_I}{\partial P_1} & \frac{\partial T_I}{\partial P_2} & \frac{\partial T_I}{\partial P_3}\end{pmatrix} \tag{11}$$

The Jacobian $\vec{\vec{J}}^k$ is approximated with a finite difference approximation [14]. For example, the sensitivity coefficient is given by:

$$J_{ij}=\frac{\partial \hat{T}_i}{\partial P_j}\cong\frac{\hat{T}\left(t_i\,;P_1,...,P_j+\left(\delta P_j\right),...P_N\right)}{2\left(\delta P_j\right)} - \frac{\hat{T}\left(t_i\,;P_1,...,P_j-\left(\delta P_j\right),...P_N\right)}{2\left(\delta P_j\right)} \tag{12}$$

The parameter perturbation $\left(\delta P_j\right)$ is set to $\xi\left(1+\left|P_j\right|\right)$, where ξ is a small number. The subscripts *i* and *j* represent the time and the parameter respectively.

In order to reduce the computational effort, the Jacobian matrix is updated using BM [20].

For the first iteration, for every *2*N* iterations and for iterations where $\Psi\left(P+\Delta P\right)>\Psi\left(P\right)$, the sensitivity coefficients of the Jacobian matrix are estimated with (12). For every other iteration, the Jacobian matrix is updated with the expression proposed by Broyden [20]:

$$J_k=J_{k-1}+\frac{\left(\left(\hat{T}_k-\hat{T}_{k-1}\right)-J_{k-1}\Delta P_{k-1}\right)\Delta P_{k-1}^T}{\Delta P_{k-1}^T\Delta P_{k-1}} \tag{13}$$

ΔP_{k-1} is the incremental value of the unknown parameters given by (10).

Convergence of the LMM is declared when

$$\begin{cases} J^T\left\|Y\left(t_i\right)-\hat{T}\left(t_i,\vec{P}\right)\right\|<\varepsilon_1\\ \left(\frac{P^{k+1}-P^k}{P^{k+1}}\right)<\varepsilon_2\\ \Psi\left(P^{k+1}\right)<\varepsilon_3\end{cases} \tag{14}$$

$\{\varepsilon_1;\ \varepsilon_2;\ \varepsilon_3\}$ are a small number.

The overall computational procedure using LMM and BM is as follows:

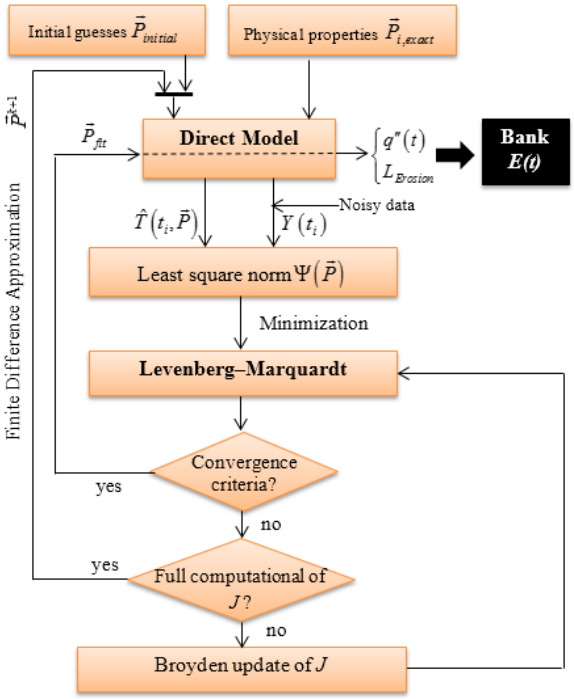

Fig. 5 Overall algorithm for the inverse method

V. Results and Discussion

The inverse procedure proposed in Fig. 5 was employed for predicting simultaneously the unknown time-varying heat flux *q*"(t) and the unknown thickness of the eroded wall $L_{Erosion}$ (Fig. 4).

Once the heat flux *q*"(t) and the thickness of the eroded refractory wall $L_{Erosion}$ are estimated, the bank *E(t)* is easily determined from the FVM presented in Section II above.

The temperatures measurements Y_i were taken with a sensor located inside the brick wall at two different locations: The first position, called '*Sensor#1*', is near the outside surface of the brick wall. The second position, '*Sensor#2*', is in the middle of the brick wall (Fig. 4).

The data-capture-frequency (the total number of temperature recordings during an experiment, t=0 to 400000 s) is *I*=800.

In order to assess the accuracy and the uniqueness of the inverse analysis, the inverse procedure has been thoroughly tested with noisy measurements and for different positions of the embedded sensor.

In order to mimic measurement errors, a random error noise $\vec{\omega}_i$ is added to the exact temperature $\vec{T}_{exact}$ generated by the direct model:

$$\vec{T}\left(t_i\right)=\vec{T}_{exact}\left(t_i\right)+\sigma\vec{\omega}_i \tag{15}$$

σ is the standard deviation of the measurement errors, which may take the value of 2% T_{max} and 4% T_{max}. T_{max} is the maximum temperature measured by the sensor.

To demonstrate the accuracy of the present inverse method for predicting the bank thickness, two cases (different heat flux q"(t)) were examined:

heat flux at $x=L_{Brick} + L_{PCM}$

Case#1 $$q''(t) = P_1 + P_2 * \sin^2\left(\frac{2\pi . t}{t_{\max}}\right)$$

Case#2 $$q''(t) = P_1 + P_2 * \left(1 - \exp\left(-\frac{t}{t_{\max}}\right)\right)$$

The exact values for the direct model, are $P_{exact} = \{P_1 = 9000\ [\mathrm{w/m^2}]\ ;\ P_2 = 8000[\mathrm{w/m^2}]\}$

For the sake of comparing the inverse solution (inverse model) to the exact solution (direct model), two estimation errors are defined:

$$\mathrm{Error}_{E(t)} = \frac{\left|E(t_i)_{inverse} - E(t_i)_{exact}\right|}{\left|E(t_i)_{exact}\right|} \quad (16)$$

$$Error_P\ \% = 100 \times \frac{\left|P_{inverse} - P_{exact}\right|}{\left|P_{exact}\right|} \quad (17)$$

Table II illustrates the effect of the sensor location on the estimation of the unknown parameters. It is seen that the relative errors vary from 0 to 10,5%. The largest discrepancy, i.e., 10,5%, occurs in the prediction of P_3 (the erosion thickness). P_3 is the smallest and therefore the most sensitive parameter [21]. It is observed that sensor#2 provides the best parameter estimation.

Figs. 6 and 7 compare the measured noisy temperatures (generated with the 1-D direct model with noise of 2% T_{max}) to the estimated temperatures predicted by the inverse model using sensor#1.

TABLE II
EFFECT OF THE SENSOR LOCATION

			Sensor#1		Sensor#2	
		P_{Exact}	$P_{Inverse}$	$Error_P$	$P_{Inverse}$	$Error_P$
Case 1	P_1 (W/m^2)	9000	9065,7	0,7	9065,4	0,7
	P_2 (W/m^2)	8000	7896,7	1,3	7898,2	1,3
	P_3 (mm)	10	9,27	7,3	9,31	6,9
Case 2	P_1 (W/m^2)	9000	8999,5	0,0	8983,1	0,2
	P_2 (W/m^2)	8000	8035,5	0,4	8018,6	0,2
	P_3 (mm)	10	8,95	10,5	9,14	8,6

Figs. 8 and 9 show the effect of the noise level on the predicted time-varying thickness of the protective bank $E(t)$ for both cases. The erosion of the refractory brick wall is depicted by the negative bank thickness. As expected, a slight discrepancy appears when the noise level increase from 2% T_{max} to 4% T_{max}. Nevertheless, it is seen that the predictions remain stable and accurate even for noisy signals.

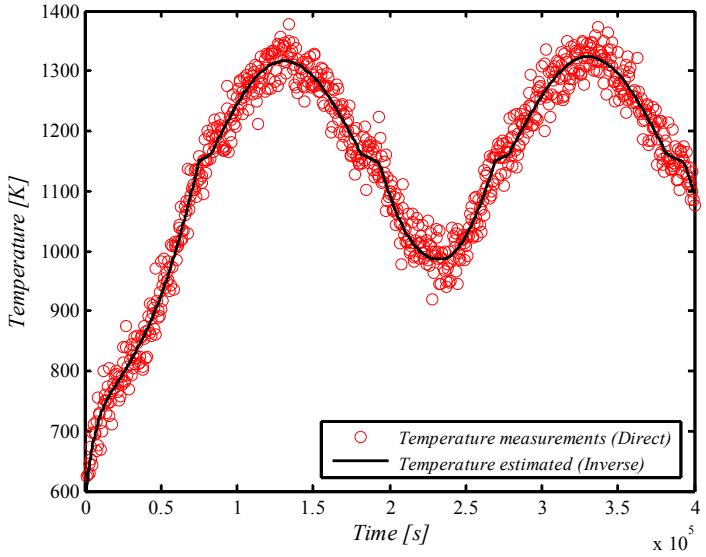

Fig. 6 Measurements and inverse predictions (Case#1)

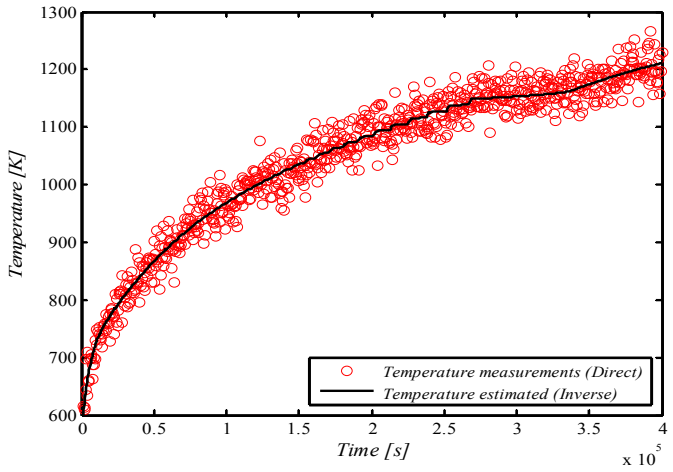

Fig. 7 Measurements and inverse predictions (Case#2)

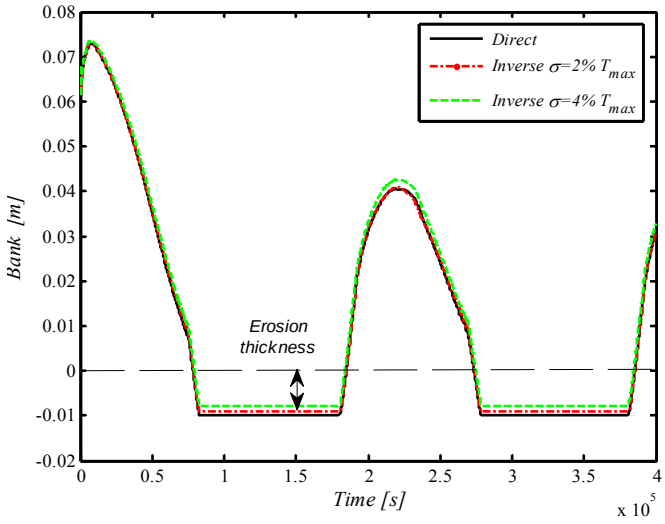

Fig. 8 Predicted bank thickness with erosion (Case#1)

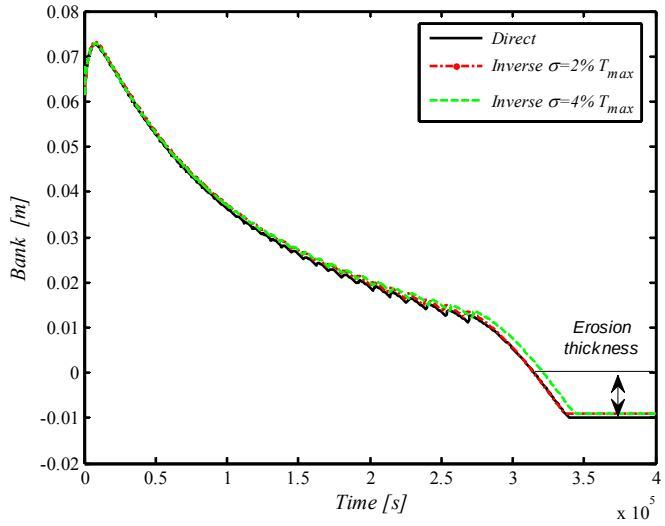

Fig. 9 Predicted bank thickness with erosion (Case#2)

Figs. 10 and 11 show the effect of the temperature sensor position (sensor#1 and sensor#2) on the accuracy of the predicted bank thickness *E(t)*. It is seen that the effect of the sensor position is insignificant [7]. Therefore, sensor#1 is recommended over sensor#2. This result is of interest to the process industry. Indeed, it is much safer and easier to embed a sensor near the external surface of the refractory brick wall.

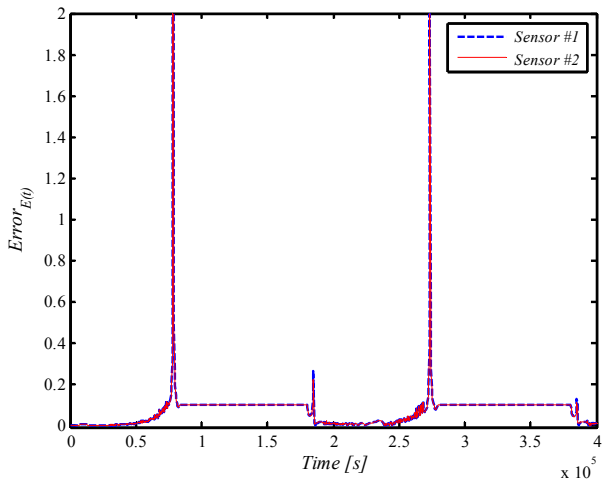

Fig. 10 Effect of the sensor position on the predicted bank thickness *E(t)*, case 1

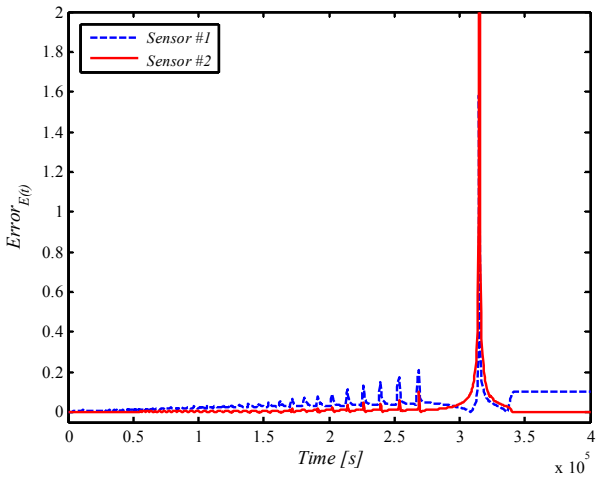

Fig. 11 Effect of the sensor position on the predicted bank thickness *E(t)*, case 2

It is noted that the approximation of the sensitivity coefficients of the Jacobian matrix, (12), requires the solution of the direct problem six times per iteration (2 times for each unknown parameter). As a result, the finite difference approximation is computationally expensive.

In order to reduce the computation time, the sensitivity matrix was updated using BM [20]. This strategy has been applied successfully in the field of inverse heat transfer problems (IHTP) [22]-[24].

LMM combined with BM (LMM/BM) calls the direct model 20 times while LMM requires 35 calls. Consequently, the CPU time for the LMM/BM is only 715,5 s while that for the LMM is 1311,9 s.

The simulations were executed with the MATLAB software running on an Intel ® Core(TM) i5-2520M CPU @ 2,50GHz.

VI. Conclusion

An inverse heat transfer analysis was presented for predicting the wall erosion and the time-varying thickness of the protective bank inside a melting furnace. It was shown that the inverse analysis may also predict simultaneously the time-varying heat flux and the eroded portion of the refractory brick wall. The proposed inverse method rests on the LMM/BM. Using this combination of methods, the computation time was halved. The effect of the measurement noise and of the location of the temperature sensors on the inverse predictions was investigated. Recommendations were made concerning the location of the sensor embedded in the brick wall. Finally, this study illustrates how the inverse heat transfer can be used successfully for preventive maintenance of an industrial facility.

Acknowledgment

The authors are grateful to the Natural Sciences and Engineering Research Council of Canada (NSERC) for their financial support.

Nomenclature

C_p	specific heat [J/kg K]
dt	time step [s]
f	liquid fraction
h	heat transfer coefficient [W/m^{2}K]
I	total number of measurements
J	Jacobian matrix
k	thermal conductivity [W/m K]
L_{Brick}	width of the brick wall [m]
$L_{Erosion}$	width of the erosion [m]
L_{PCM}	width of the PCM layer [m]
N	number of unknown parameters
$q^{"}(t)$	heat flux [W/m^2]
P	vector of unknown parameter
PCM	phase change material
$Error$	estimation errors [%]
$E(t)$	bank thickness [m]
t	time [s]
$\hat{T}$	estimated temperature [K]
x	Cartesian spatial coordinate [m]
Y	measured temperature [K]
ε	small number
μ	damping parameter
ρ	density [kg/m^3]
σ	standard deviation of the measurement error
ψ	sum of squares norm
ξ	small number

δH	enthalpy [J/m^3]
Δ	difference
Ω^k	diagonal matrix
λ	heat of fusion [J/kg]
ω	random number

A. Subscripts

0	initial value
∞	ambiant
$Brick$	brick wall
$Exact$	exact solution
$E(t)$	bank thickness
liq	liquidus
$liquid$	liquid (PCM)
max	maximum
PCM	phase change material
$q''(t)$	heat flux
sol	solidus
$solid$	solid (PCM)

B. Superscripts

k	time iteration number
T	transposed matrix
$\hat{}$	estimated parameter
$\vec{}$	vector
$\bar{\bar{}}$	matrix

REFERENCES

[1] M. A. Marois, M. Désilets, and M. Lacroix, Prediction of a 2-D Solidification Front in High-Temperature Furnaces by an Inverse Analysis, Numer. Heat Transfer A, vol. 59, no. 3, pp. 151–166, 2011.

[2] M. LeBreux, M. Désilets, and M. Lacroix, Fast Inverse Prediction of Phase Change Banks in High-Temperature Furnaces with a Kalman Filter Coupled with a Recursive Least-Square Estimator, Int. J. of Heat and Mass Transfer, vol. 53, no. 23–24, pp. 5250–5260, 2010.

[3] M. LeBreux, M. Désilets, and M. Lacroix, An unscented Kalman filter inverse heat transfer method for the prediction of the ledge thickness internal high-temperature metallurgical reactors, Int. J. of Heat and Mass Transfer, vol. 57, no. 1, pp. 265-273, 2013.

[4] M. LeBreux, M. Désilets, and M. Lacroix, Control of the Ledge Thickness in High-Temperature Metallurgical Reactor using a Virtual Sensor, Inverse Problems in Sci. and Eng., vol. 20, no. 8, pp. 1215–1238, 2012.

[5] M. LeBreux, M. Désilets, and M. Lacroix, Prediction of the Time-Varying Ledge Profile internal a High-Temperature Metallurgical Reactor with an Unscented Kalman Filter-Based Virtual Sensor, Numer. Heat Transfer A, vol. 64, pp. 551-576, 2013.

[6] M. LeBreux, M. Désilets, and M. Lacroix, Is the performance of a virtual sensor employed for the prediction of the ledge thickness internal a metallurgical reactor affected by the thermal contact resistance?, WIT Transactions on Eng. Sci. , Vol. 83, pp. 517-526, 2014.

[7] O. Tadrari and M. Lacroix, Prediction of Protective Banks in High-Temperature Smelting Furnaces by Inverse Heat Transfer, Int. J. of Heat and Mass Transfer, vol. 49, no. 13–14, pp. 2180–2189, 2006.

[8] M. A. Marois, M. Désilets, and M. Lacroix, Prediction of the Bank Formation in High Temperature Furnaces by a Sequential Inverse Analysis with Overlaps, Numer. Heat Transfer A, vol. 60, pp. 561–579, 2011.

[9] M. A. Marois, M. Désilets, and M. Lacroix, What is the Most Suitable Fixed Grid Solidification Method for Handling Time-Varying Inverse Stefan Problems in High Temperature Industrial Furnaces?, Int. J. of Heat and Mass Transfer, vol. 55, pp. 5471–5478, 2012.

[10] C. Bertrand, M. A. Marois, M. Désilets, G. Soucy, and M. Lacroix, A combined 2D inverse predictions and experimental analysis for the bank formation internal a metallurgical reactor, Int. J. of Heat and Mass Transfer, vol. 59, pp. 58-65, 2013.

[11] Y. Zhang, R. Deshpande, D. F. Huang, P. Chaubal, and C. Q. Zhou, Numerical analysis of blast furnace hearth inner profile by using CFD and heat transfer model for different time periods, Int. J. of Heat and Mass Transfer, vol. 51, nos. 1–2, pp. 186–197, 2008.

[12] C.M. Chang, W.T. Cheng, C.E. Huang and S.W. Du, Numerical prediction on the erosion in the hearth of a blast furnace during tapping process, Int. J. of Heat and Mass Transfer, vol. 36, no. 5, pp. 480–490, 2009.

[13] V. Guillaume, L. Gosselin, and M. Lacroix, an enhanced thermal conduction model for the prediction of convection dominated solid–liquid phase change, Int. J. of Heat and Mass Transfer, vol. 52, no. 7-8, pp. 1753-1760, 2009.

[14] M. N. Ozisik and H. R. B. Orlande, Inverse Heat Transfer: Fundamentals and Applications, Taylor and Francis, New York, 2000.

[15] V. R. Voller, Development and application of a heat balance integral method for analysis of metallurgical solidification, Applied Mathematical Modelling, pp. 3-11, 1989.

[16] V. R. Voller and C. R. Swaminathan, General Source-Based Method for Solidification Phase Change, Numer. Heat Transfer, vol. 19, pp. 175–189, 1991.

[17] A.M. Guzmán, D.I. Martínez and R. González, Corrosion–erosion wear of refractory bricks in glass furnaces, Engineering Failure Analysis, Vol. 46, pp. 188–195, 2014.

[18] M. Kaur, H. Singh, and S. Prakash, Surface engineering analysis of detonation-gun sprayed Cr3C2–NiCr coating under high-temperature oxidation and oxidation–erosion environments, Surface and Coatings Technology, vol. 206, no. 2–3,pp. 530–541, 2011.

[19] D. W. Marquardt, An algorithm for least-squares estimation of nonlinear parameters, J. of the Society for Industrial and Applied Mathematics, pp. 431-441, 1963.

[20] C. G. Broyden, A class of methods for solving nonlinear simultaneous equations, Mathematics of computation, pp. 577-593, 1965.

[21] B. Sawaf, and M. N. Özisik, Determining the constant thermal conductivities of orthotropic materials by inverse analysis, Int. communications in heat and mass transfer, vol. 22, no. 2, pp. 201-211, 1995.

[22] B. Moghadassian, and F. Kowsary, Inverse boundary design problem of natural convection–radiation in a square enclosure, Int. J. of Thermal Sci. vol. 75, pp. 116-126, 2014.

[23] K. W. Kim, and S. W. Baek, Inverse radiation–conduction design problem in a participating concentric cylindrical medium, Int. J. of Heat and Mass Transfer, vol. 50, no. 13-14, pp. 2828-2837, 2007.

[24] M. Hafid and M. Lacroix, Prediction of the Thermal Parameters of a High-Temperature Metallurgical Reactor Using Inverse Heat Transfer, Int. J. of Mechanical, Aerospace, Industrial, Mechatronic and Manufacturing Engineering, vol. 10, no 6, pp. 907-913, 2016.